pp 1523–1544.
doi:10.1017/aer.2020.26

Turbo-electric propulsive fuselage aircraft BLI benefits: A design space exploration using an analytical method

P. Giannakakis, C. Pornet and A. Turnbull
panagiotis.giannakakis@safrangroup.com
Energy and Propulsion
Safran Tech
Châteaufort
France

ABSTRACT

Turbo-electric propulsive fuselage aircraft featuring Boundary-Layer Ingestion (BLI) are considered promising candidates to achieve the emissions reduction targets set for aviation. This paper presents an analytical method capable of estimating the BLI benefit at aircraft level, enabling a quick exploration of the propulsive fuselage design space. The design space exploration showed that the assumptions regarding the underwing turbofans and BLI fan mass estimation can have an important impact on the final fuel burn estimation. The same applies to the total efficiency assumed for the electric transmission, the range of the aircraft mission, and the propulsive efficiency of the engines used as benchmark. The regional jet and short- to medium-range aircraft classes seem to be the most promising as the ingested drag and power saving are among the largest, with long-range aircraft being just behind. The future introduction of advanced technologies, which target the reduction of vortex and wave dissipation at aircraft level, could increase the potential benefit of propulsive fuselage BLI. On the other hand, the potential benefit would be decreased if more efficient and lighter ultra high bypass ratio engines were used as benchmark.

Keywords: Boundary-layer ingestion; Propulsion; Turbo-electric; Performance evaluation

NOMENCLATURE

A_{BLIF}	BLI propulsor inlet section (m^2)
BPR	turbofan bypass ratio
C_{Dp}	profile drag coefficient
C_{Di}	lift-induced drag coefficient

Received 16 October 2019; revised 24 February 2020; accepted 3 March 2020.

C_{Dw}	wave drag coefficient
C_D	total drag coefficient
D_{BLIF}	BLI propulsor inlet tip diameter (m)
$D_{\mathrm{BLIF},hub}$	BLI propulsor inlet hub diameter (m)
FB	fuel burn (kg)
f	ingested viscous dissipation relative to total dissipation
h_{BLIF}	BLI propulsor inlet height (m)
H	boundary-layer shape factor, $= \frac{\delta^*}{\theta}$
H^*	boundary-layer kinetic energy shape factor, $= \frac{\theta^*}{\theta}$
M	propulsive system mass (kg)
MFR	mass flow ratio, $\frac{A_0}{A_{\mathrm{BLIF}}}$, A_0 being the area before the pre-compression zone
$\dot{m}$	mass flow (kg/s)
P_{core}	power available at engine core exit (W)
P_K	conventional propulsor output mechanical energy (W)
PSC	power saving coefficient, $\frac{P_K - P'_K}{P_K}$
q	BLI propulsor power/thrust relative to total power/thrust, $q = \Phi'_{\mathrm{BLIF}}/\Phi'$
TSFC	thrust specific fuel consumption (kg/s/N)
$\mathrm{S_W}$	propulsive system wetted surface ($\mathrm{m^2}$)
SMR	short-to-medium range
SP_e	electric transmission specific power (kW/kg)
V_0	free-stream velocity (m/s)
V_e	boundary-layer edge velocity (m/s)
V_{jet}	jet velocity (primary and secondary flows average for a turbofan) (m/s)
u	air velocity in the boundary-layer (m/s)
$\mathrm{XR_M}$	mass exchange rate (%FB/1,000kg)
$\mathrm{XR_S}$	wetted surface exchange rate (%FB/10 $\mathrm{m^2}$)
$\mathrm{XR_{TSFC}}$	TSFC exchange rate (%FB/%TSFC)

Greek symbol

α	total propulsion system inlet mass flow ratio $= \frac{\dot{m}'}{\dot{m}}$
α_{BLIF}	BLI propulsor mass flow ratio $= \frac{\dot{m}'_{\mathrm{BLIF}}}{\dot{m}'}$
β	ingested viscous dissipation relative to total viscous dissipation
$\beta_{fuselage}$	fuselage viscous dissipation relative to total viscous dissipation
$\delta,\ \delta^*$	boundary-layer thickness and displacement thickness (m)
ΔKE	kinetic energy defect (W)
η_e	electric transmission efficiency
η_{fan}	fan isentropic efficiency
η_{LPT}	low-pressure turbine isentropic efficiency
η_{pr}	propulsive efficiency
η_{tr}	transmission efficiency
$\theta,\ \theta^*$	boundary-layer momentum and kinetic energy thicknesses (m)

https://doi.org/10.1017/aer.2020.26 Published online by Cambridge University Press

λ	the sum of vortex and wave dissipation relative to viscous dissipation
ρ	density (kg/m^3)
ψ	viscous dissipation upstream of the propulsor relative to non-BLI case
Φ	total aircraft dissipation (W)
Φ_{jet}	jet dissipation (W)
Φ_p	profile mechanical energy dissipation (W)
Φ_{vortex}	vortex dissipation (W)
Φ_{wave}	shock wave dissipation (W)

Superscript

$()'$	quantity of the BLI configuration

Subscript

ext.	external (non-ingested) quantity
int.	internal (ingested) quantity
TF	non-BLI turbofan quantity
BLIF	BLI fan quantity

1.0 INTRODUCTION

Boundary-Layer Ingestion (BLI) is considered a potential technological enabler for achieving the carbon dioxide emissions reduction goals set for aviation by the Advisory Council for Aviation Research and Innovation in Europe (ACARE)[1]. A propulsive fuselage tube-and-wing concept using a fan encircling the rear of the fuselage, ingesting all or a part of the fuselage boundary-layer, is considered to be one of the most promising candidates[2]. By ingesting the fuselage boundary-layer, an improvement in propulsive efficiency and a reduction in fuselage wake dissipation can be achieved. The BLI fan can either be powered by a dedicated gas turbine[2], or by using electricity generated by the underwing turbofans in a partial turbo-electric configuration, e.g. such as the STARC-ABL aircraft[3]. Specifically for the turbo-electric configuration, different studies claim fuel burn changes that range from -3.4%[4] to $+0.5\%$[5], while another work by the authors estimated $+1.7 \pm 1\%$[6]. This work tries to shed light on the parameters that drive the estimated fuel burn change in order to explain the variance found in the literature results.

Due to the strong aero-propulsive integration, conventional thrust-drag book-keeping methods cannot be applied to quantify the benefits. Consequently, an energy-based analytical method was developed in order to assess the BLI potential benefit during conceptual design. The method relies on the power balance approach developed by Drela[7] and subsequently applied on a hybrid-wing-body by Sato[8], and on the D8 aircraft by Hall et al[9] and Uranga et al[10]. In this paper, the method has been extended in order to assess the BLI benefit of propulsive fuselage tube-and-wing aircraft, similar to the work of Hall et al[5]. The analytical method also covers the integration of the fuselage fan propulsion system at aircraft level in order to explore the design space in terms of fuel burn.

https://doi.org/10.1017/aer.2020.26 Published online by Cambridge University Press

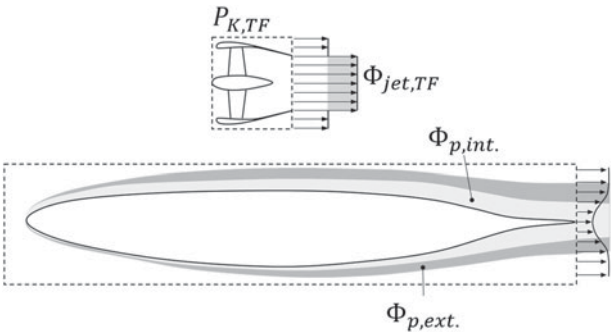

Figure 1. Illustration of the baseline aircraft power terms for the fuselage and propulsor.

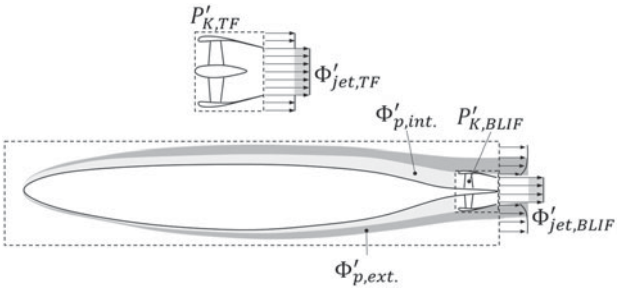

Figure 2. Propulsive fuselage aircraft power terms.

The approach is applied to a short-to-medium range (SMR) tube-and-wing aircraft to evaluate the fuel burn reduction potential of a partial turbo-electric propulsion system featuring fuselage BLI. Furthermore, a design space exploration identifies the conditions that need to be met in order to achieve meaningful fuel burn reductions. Finally, an aircraft sensitivity analysis is conducted to determine the potential of ingesting the complete fuselage boundary-layer for different aircraft applications, from the perspective of aircraft size and mission type.

2.0 METHOD DEVELOPMENT

2.1 Power saving estimation method

The power saving coefficient (PSC), first introduced by Smith[11], is defined as the reduction of the mechanical power P_K required by the propulsion system due to the ingestion of the boundary-layer. The mechanical power P_K is defined as the increase in kinetic energy through the propulsor, as shown by Equation (1) for a conventional propulsor.

$$P_K = \frac{1}{2}\dot{m}\left(V_{jet}^2 - V_0^2\right). \quad \ldots(1)$$

The analytical method is developed by applying the power balance method[7], on the conventional aircraft configuration illustrated in Fig. 1, and on the generic propulsive fuselage configuration represented in Fig. 2.

https://doi.org/10.1017/aer.2020.26 Published online by Cambridge University Press

It is noted that primed variables refer to the propulsive fuselage configuration. The implementation of the power balance method presented below has been inspired by Sato's work on a hybrid-wing-body aircraft[8] and Hall et al's work on the D8 aircraft[9].

The power balance equation[7] establishes the equilibrium between the power produced by the engine P_K and the different dissipation terms, corresponding to profile, vortex, jet, and wave drag losses, as shown in Equation (2).

$$P_K - \Phi_{jet} = \Phi = \Phi_p + \Phi_{vortex} + \Phi_{wave}. \quad \ldots (2)$$

The energy dissipation Φ'_p caused by shear stress losses on the body surface, i.e. in the boundary-layer, and in the wake of the propulsive fuselage configuration, can be split into the internal (ingested) and external part as shown by Fig. 2 and Equation (3). Although, there is no ingestion in the baseline configuration of Fig. 1 the same break-down can be applied on Φ_p; in that case the ingested part $\Phi_{p,int.}$, is the one that would be ingested if there was a propulsive fuselage.

$$\Phi'_p = \Phi'_{p,int.} + \Phi'_{p,ext.}. \quad \ldots (3)$$

At this point, one can introduce the following ratios:

$$\beta = \frac{\Phi_{p,int.}}{\Phi_p}, \quad \ldots (4)$$

$$\psi = \frac{\Phi'_{p,int.}}{\Phi_{p,int.}}. \quad \ldots (5)$$

The β ratio represents the amount of the ingested viscous dissipation relative to the total viscous dissipation of the baseline. The ψ ratio corresponds to the dissipation occurring upstream of the propulsive fuselage propulsor, relative to the total dissipation that would occur inside the ingested stream-tube if there was no BLI. For a propulsor located at the trailing edge of the fuselage, the numerator is equal to the ingested part of the dissipation occurring on the fuselage surface $\Phi_{p,surf}$[8], which is assumed unchanged between the conventional and the propulsive fuselage configurations[1]. The denominator would be the dissipation that would occur on the surface and in the wake of the stream-tube if this was not ingested. By introducing the above assumptions and definitions into Equation (3), and by considering that the dissipation that is not ingested remains unchanged ($\Phi'_{p,ext.} = \Phi_{p,ext.}$), one derives the following equation:

$$\Phi'_p = \Phi_p \left[1 - \beta \left(1 - \psi\right)\right]. \quad \ldots (6)$$

The above equation can be translated into total dissipation terms by introducing the parameters λ and f, which represent respectively the ratio of wave and vortex dissipation to the total profile dissipation (Equation (7)), and the ratio of ingested dissipation to the total aircraft

[1]This assumption is required for the derivation of a simple analytical equation, as in reality the propulsor can modify the nearby upstream flow. The quantification of these interaction dissipation terms is outside the scope of this paper as it would require a higher-fidelity CFD calculation.

https://doi.org/10.1017/aer.2020.26 Published online by Cambridge University Press

dissipation (Equation (9)). More specifically, Equation (7) is introduced in the first part of Equation (8), in order to express the total dissipation as a function of the profile dissipation and λ. Introducing Equation (6) into the left part of Equation (8) and assuming that the wave and vortex dissipation remain unchanged between the BLI and conventional configurations, Equation (10) is obtained.

$$\lambda = \frac{\Phi_{vortex} + \Phi_{wave}}{\Phi_p}, \quad \ldots(7)$$

$$\Phi = \Phi_p + \Phi_{vortex} + \Phi_{wave} = \Phi_p\,(1+\lambda)\,, \quad \ldots(8)$$

$$f = \frac{\Phi_{p,int.}}{\Phi} = \frac{\beta}{1+\lambda}, \quad \ldots(9)$$

$$\Phi' = \Phi\,[1 - f\,(1-\psi)]\,. \quad \ldots(10)$$

The power-saving coefficient is defined as follows:

$$\mathrm{PSC} = 1 - \frac{P'_K}{P_K}, \quad \ldots(11)$$

where P'_K is the propulsive power of the BLI configuration. As implied by the above equation, a positive PSC corresponds to a reduction in the required propulsive power.

Using the power balance method the propulsive efficiency is defined as the net propulsive power (taking the total power and subtracting the jet dissipation which is related to the propulsor), divided by the total propulsive power[8,9], Equation (12).

$$\eta_{pr} = \frac{P_K - \Phi_{jet}}{P_K}. \quad \ldots(12)$$

By introducing the propulsive efficiency definition, PSC is derived in Equation (13).

$$\mathrm{PSC} = 1 - \frac{P'_K - \Phi'_{jet}}{P_K - \Phi_{jet}}\frac{\eta_{pr}}{\eta'_{pr}}. \quad \ldots(13)$$

Combining Equation (13) with Equations (2) and (10) gives:

$$\mathrm{PSC} = 1 - [1 - f\,(1-\psi)]\,\frac{\eta_{pr}}{\eta'_{pr}}, \quad \ldots(14)$$

where η'_{pr} is the propulsive efficiency of the BLI configuration.

The above equation clearly shows that part of the power saving comes from the propulsive efficiency improvement and part from the aircraft dissipation reduction; i.e. even without an increase in propulsive efficiency, the BLI can produce a power saving due to the reduction of the aircraft mechanical energy dissipation. The power saving increases for increasing BLI, as this increases β and f. For a given β, the power saving increases when the wave and induced drag represent a smaller share of total drag, leading to a lower λ and higher f. Steiner et al[12] also reached to a similar conclusion in their study. In a case without wave and induced drag ($f = \beta$), where all the boundary-layer is ingested by a propulsor located on the trailing

https://doi.org/10.1017/aer.2020.26 Published online by Cambridge University Press

edge, and assuming no change in propulsive efficiency, the power saving coefficient is equal to $(1-\psi)$; i.e. a higher wake dissipation relative to the surface dissipation, leads to a lower ψ, and a higher power saving. As shown by Hall[13] in a similar analysis, the ψ parameter is half the kinetic energy shape factor, $\psi = \frac{H^*}{2}$, which for a typical attached turbulent flow gives a value of around $\psi = 0.875$[7]. For such a case, the above assumptions would result in a PSC of 12.5%.

Until now, no assumption was made with respect to the system architecture. In order to calculate the propulsive efficiency change, the rest of the paper will focus on the propulsive fuselage configuration shown in Fig. 2 as compared to the baseline of Fig. 1.

Writing the power balance equation (Equation (2)) for the tube-and-wing baseline gives:

$$P_K - \Phi_{jet} = \dot{m} V_0 \left(V_{jet} - V_0\right) = \Phi. \qquad \ldots (15)$$

The propulsive efficiency is defined as follows:

$$\eta_{pr} = \frac{P_K - \Phi_{jet}}{P_K} = \frac{2V_0}{V_{jet} + V_0} = \frac{2}{V_{jet}/V_0 + 1}. \qquad \ldots (16)$$

By introducing the power split ratio[2] $q = \Phi'_{\mathrm{BLIF}}/\Phi'$, the power balance of the turbofans represented in Fig. 2 is written as:

$$\begin{aligned} P'_{K,\mathrm{TF}} - \Phi'_{jet,\mathrm{TF}} &= \overbrace{\frac{1}{2}\dot{m}'_{\mathrm{TF}}\left(V'^2_{jet,\mathrm{TF}} - V_0^2\right)}^{P'_{K,\mathrm{TF}}} - \frac{1}{2}\dot{m}'_{\mathrm{TF}}\left(V'_{jet,\mathrm{TF}} - V_0\right)^2 = \dot{m}'_{\mathrm{TF}} V_0 \left(V'_{jet,\mathrm{TF}} - V_0\right) \\ &= (1-q)\,\Phi' = (1-q)\,\Phi\left[1 - f\,(1-\psi)\right]. \end{aligned} \qquad \ldots (17)$$

Combining Equations (17) and (15) gives the following expression for the turbofan jet velocity of the propulsive fuselage BLI configuration:

$$\frac{V'_{jet,\mathrm{TF}}}{V_0} = \frac{(1-q)\left[1 - f\,(1-\psi)\right]}{\alpha\,(1-\alpha_{\mathrm{BLIF}})}\left(\frac{V_{jet}}{V_0} - 1\right) + 1, \qquad \ldots (18)$$

where α is the ratio of total propulsor mass flow for the BLI configuration relative to the total propulsor mass flow of the conventional non-BLI baseline:

$$\alpha = \frac{\dot{m}'}{\dot{m}} = \frac{2\dot{m}'_{\mathrm{TF}} + \dot{m}'_{\mathrm{BLIF}}}{2\dot{m}_{\mathrm{TF}}}, \qquad \ldots (19)$$

and α_{BLIF} is the ratio of BLI propulsor fan mass flow to total propulsor mass flow for the BLI configuration:

$$\alpha_{\mathrm{BLIF}} = \frac{\dot{m}'_{\mathrm{BLIF}}}{\dot{m}'}. \qquad \ldots (20)$$

[2] Φ'_{BLIF} being the part of the total aircraft dissipation for which the BLI fan is sized.

https://doi.org/10.1017/aer.2020.26 Published online by Cambridge University Press

Similarly, the power balance of the BLI fan of the configuration presented in Fig. 2 is written as:

$$P'_{K,\mathrm{BLIF}} - \Phi'_{jet,\mathrm{BLIF}} = \overbrace{\frac{1}{2}\dot{m}'_{\mathrm{BLIF}}\left(V'^{2}_{jet,\mathrm{BLIF}} - V_0^2\right) + \beta\psi\Phi_p}^{P'_{K,\mathrm{BLIF}}} - \frac{1}{2}\dot{m}'_{\mathrm{BLIF}}\left(V'_{jet,\mathrm{BLIF}} - V_0\right)^2$$
$$= q\Phi\left[1 - f\left(1-\psi\right)\right]. \quad \ldots(21)$$

The term $\beta\psi\Phi_p$ corresponds to the mechanical power loss between the free-stream V_0 and the inlet of the BLI fan. The above equation is subsequently combined with Equation (15) to obtain the following expression for the propulsive fuselage BLI fan jet velocity:

$$\frac{V'_{jet,\mathrm{BLIF}}}{V_0} = \frac{q\left[1 - f\left(1 - \psi\frac{q-1}{q}\right)\right]}{\alpha\alpha_{\mathrm{BLIF}}}\left(\frac{V_{jet}}{V_0} - 1\right) + 1. \quad \ldots(22)$$

The propulsive efficiency of the propulsive fuselage configuration is given by the following equation:

$$\eta'_{pr} = \frac{P'_{K,\mathrm{TF}} - \Phi'_{jet,\mathrm{TF}} + P'_{K,\mathrm{BLIF}} - \Phi'_{jet,\mathrm{BLIF}}}{P'_{K,\mathrm{TF}} + P'_{K,\mathrm{BLIF}}}. \quad \ldots(23)$$

Using the definitions of P_K and Φ_{jet}, in the same way as for Equations (17) and (21), the following equation is obtained for the propulsive efficiency of the propulsive fuselage configuration:

$$\eta'_{pr} = \frac{A}{\frac{V'_{jet,\mathrm{BLIF}}+V_0}{2V_0}qB + \frac{V'_{jet,\mathrm{TF}}+V_0}{2V_0}\left(1-q\right)A + f\psi}, \quad \ldots(24)$$

$$A = 1 - f\left(1-\psi\right), \quad \ldots(25)$$

$$B = 1 - f\left(1 - \psi\frac{q-1}{q}\right). \quad \ldots(26)$$

Equations (24) and (16) can now be combined with Equation (14) to calculate the power saving coefficient:

$$\mathrm{PSC} = 1 - \frac{\left(\frac{V'_{jet,\mathrm{BLIF}}}{V_0} + 1\right)qB + \left(\frac{V'_{jet,\mathrm{TF}}}{V_0} + 1\right)\left(1-q\right)A + 2f\psi}{\frac{V_{jet}}{V_0} + 1}. \quad \ldots(27)$$

The above equation is applicable to a BLI configuration, where the BLI fan provides a part ($q < 1$), or all of the propulsive power ($q = 1$). In this case, Equation (27) reduces to the following simpler expression:

https://doi.org/10.1017/aer.2020.26 Published online by Cambridge University Press

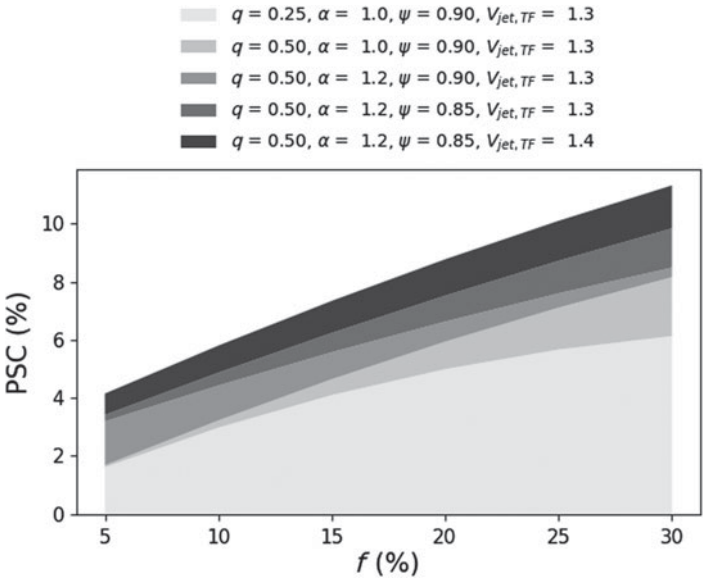

Figure 3. Sensitivity of PSC to different input parameters.

$$\mathrm{PSC} = 1 - \frac{\left(\frac{V'_{jet,\mathrm{BLIF}}}{V_0} + 1\right)(1-f) + 2f\psi}{\frac{V_{jet}}{V_0} + 1}. \qquad \ldots (28)$$

The sensitivity of PSC against the parameters q, ψ, α, and $\frac{V_{jet}}{V_0}$ is evaluated for a variation of f in Fig. 3. The relation between PSC and f indicates that the larger the f value, the higher the potential BLI benefits. With increasing q, more thrust is produced by the more efficient BLI propulsor and as a result PSC increases. By decreasing ψ, less dissipation occurs ahead of the propulsor leading to an increase in PSC. According to Equations (18) and (22), a larger value of α results in a decrease in the jet velocities of the propulsion system, which results in a higher propulsive efficiency and a BLI gain. Finally, for a given q, a variation of $\frac{V_{jet}}{V_0}$ reflects a change in the propulsive efficiency of the baseline propulsors. Deteriorating the propulsive efficiency of the baseline configuration by increasing $\frac{V_{jet}}{V_0}$ results in a higher PSC and BLI benefit.

In Equations (27) and (28), the jet velocities $V'_{jet,\mathrm{BLIF}}$ and $V'_{jet,\mathrm{TF}}$ can either be chosen directly, or indirectly by defining α and α_{BLIF} in Equations (18) and (22), as the propulsor mass flows and jet velocities are interrelated. The BLI fan mass flow is also related to the amount of boundary-layer ingested. The relation between the aforementioned mass flows, jet velocities and the BLI parameter β (and hence f) is the last missing element. The determination of this relation requires the physical sizing of the BLI propulsor[3], which is the subject of the following section.

[3]The BLI propulsor includes the fan and nacelle. However, the term BLI fan is sometimes used to signify the BLI propulsor.

https://doi.org/10.1017/aer.2020.26 Published online by Cambridge University Press

2.2 Propulsor sizing for a propulsive fuselage architecture

Assuming an axi-symmetric aircraft fuselage geometry, for given BLI fan diameter D'_{BLIF}, hub diameter $D'_{hub,\mathrm{BLIF}}$, and known inlet boundary-layer profile, the sizing starts with the calculation of the boundary-layer related parameters, i.e. the average BLI fan inlet velocity and the amount of ingested mechanical energy defect corresponding to the fuselage, Equations (29)–(31). The amount of viscous aircraft mechanical energy defect ingested is then calculated by Equation (32), for a given ratio of fuselage profile drag to total profile drag. For a given ratio λ, between vortex/wave and viscous dissipation, Equation (9) gives the ratio of ingested mechanical power defect over the total aircraft power dissipation.

$$h'_{\mathrm{BLIF}} = \frac{1}{2}\left(D'_{\mathrm{BLIF}} - D'_{hub,\mathrm{BLIF}}\right), \quad \ldots(29)$$

$$V'_{inlet,\mathrm{BLIF}} = \frac{\int_0^{h'_{\mathrm{BLIF}}} \rho u^2 \left(0.5D'_{hub,\mathrm{BLIF}} + y\right)\, \mathrm{d}y}{\int_0^{h'_{\mathrm{BLIF}}} \rho u \left(0.5D'_{hub,\mathrm{BLIF}} + y\right)\, \mathrm{d}y}, \quad \ldots(30)$$

$$\beta_{fuselage} = \frac{\Delta \mathrm{KE}\left(h'_{\mathrm{BLIF}}\right)}{\Delta \mathrm{KE}\left(\delta\right)} = \frac{\int_0^{h'_{\mathrm{BLIF}}} \left(V_e^2 - u^2\right) \rho u \left(0.5D'_{hub,\mathrm{BLIF}} + y\right)\, \mathrm{d}y}{\int_0^{\delta} \left(V_e^2 - u^2\right) \rho u \left(0.5D'_{hub,\mathrm{BLIF}} + y\right)\, \mathrm{d}y}, \quad \ldots(31)$$

$$\beta = \beta_{fuselage} \frac{C_{Dp,fuselage}}{C_{Dp}}. \quad \ldots(32)$$

For a given BLI nacelle mass flow ratio (MFR), Equations (33) and (34) give the BLI fan mass flow. Subsequently, for given velocity ratio $\frac{V_{jet}}{V_0}$ and inlet mass flow of the conventional baseline, known propulsive power split q, and considering the same velocity ratio ($\frac{V'_{jet,\mathrm{TF}}}{V_0} = \frac{V_{jet}}{V_0}$) for the under-wing turbofans of the propulsive fuselage configuration, Equations (18)–(20), define the parameters α, α_{BLIF}, the total mass flow $\dot{m}'$ and the under-wing turbofan mass flow $\dot{m}'_{\mathrm{TF}}$. The BLI fan jet velocity is then calculated using Equation (22) and the power saving coefficient using Equation (27). The sizing ends by calculating the under-wing turbofan diameter, using Equations (35) and (36).

$$A'_{\mathrm{BLIF}} = \frac{\pi}{4} {D'_{\mathrm{BLIF}}}^2 \left[1 - \left(\frac{D'_{hub,\mathrm{BLIF}}}{D'_{\mathrm{BLIF}}}\right)^2\right], \quad \ldots(33)$$

$$\dot{m}'_{\mathrm{BLIF}} = \mathrm{MFR} \cdot \rho \cdot V'_{inlet,\mathrm{BLIF}} \cdot A'_{\mathrm{BLIF}}, \quad \ldots(34)$$

$$A'_{\mathrm{TF}} = \frac{\dot{m}'_{\mathrm{TF}}}{2 \cdot \mathrm{MFR} \cdot \rho \cdot V'_0}, \quad \ldots(35)$$

$$D'_{\mathrm{TF}} = \sqrt{\frac{4 \cdot A'_{\mathrm{TF}}}{\pi \cdot \left[1 - \left(\frac{D'_{hub,\mathrm{TF}}}{D'_{\mathrm{TF}}}\right)^2\right]}}. \quad \ldots(36)$$

https://doi.org/10.1017/aer.2020.26 Published online by Cambridge University Press

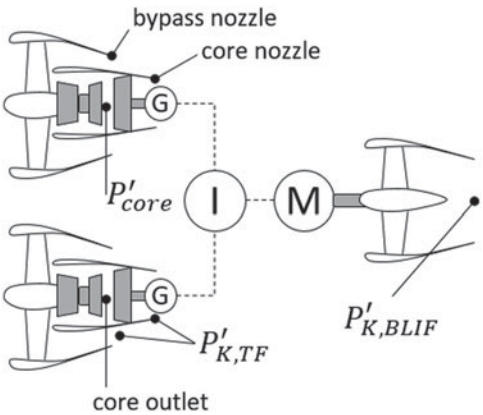

Figure 4. Simplified turbo-electric architecture including two generators, an inverter and a motor.

2.3 Fuel burn evaluation for a turbo-electric propulsive fuselage architecture

In order to estimate the BLI impact at aircraft level, the change in fuel burn needs to be calculated. Such a computation includes the change in installed propulsion system weight and drag. The whole process is presented for the partial turbo-electric propulsive fuselage architecture shown in Fig. 4, where two under-wing turbofans generate the electricity that powers the electric BLI fan.

The first step consists in translating the propulsion system kinetic energy into the energy generated by the two turbofan cores. This transformation includes: (1) the transmission losses from the BLI propulsor kinetic energy output $P'_{K,\mathrm{BLIF}}$, back to the under-wing turbofan core exit P'_{core}; (2) the transmission losses between the under-wing turbofan nozzles kinetic energy output $P'_{K,\mathrm{TF}}$, and their core exit as represented in Equation (37) using the conventional definition of the transmission efficiency. It is reminded that the conventional turbofan transmission efficiency gives the ratio between the kinetic energy delivered to the exit of the core and bypass nozzles ($P'_{K,\mathrm{TF}}$ in Fig. 4), relative to the maximum power that can be extracted from the core outlet by an ideal turbine that expands the gas to atmospheric pressure (P'_{core} in Fig. 4).

$$\eta_{tr} = \frac{P_{K,\mathrm{TF}}}{P_{core}}, \qquad \ldots (37)$$

$$P'_{core} = \frac{P'_{K,\mathrm{TF}}}{\eta_{tr}} + \frac{P'_{K,\mathrm{BLIF}}}{2 \cdot \eta_e \cdot \eta_{\mathrm{LPT,TF}} \cdot \eta'_{fan,\mathrm{BLIF}}}. \qquad \ldots (38)$$

For deriving Equation (38), the turbofan fan isentropic efficiency, $\eta_{fan,\mathrm{TF}}$, and low-pressure turbine isentropic efficiency, $\eta_{\mathrm{LPT,TF}}$, were assumed constant and equal to the baseline values for the sake of simplification. The BLI fan isentropic efficiency, $\eta'_{fan,\mathrm{BLIF}}$, can easily be related to its pressure ratio using a relation similar to the one given by Felder et al[14]. The BLI fan pressure ratio is calculated iteratively by matching the desired nozzle jet velocity $V'_{jet,\mathrm{BLIF}}$

https://doi.org/10.1017/aer.2020.26 Published online by Cambridge University Press

calculated by Equation (18). The baseline transmission efficiency can be approximated using Equation (39)[15].

$$\eta_{tr} = \frac{1 + \mathrm{BPR}}{1 + \mathrm{BPR}/(\eta_{fan,\mathrm{TF}} \cdot \eta_{\mathrm{LPT,TF}})}. \quad \ldots (39)$$

The BPR of the underwing turbofans is defined as:

$$\mathrm{BPR} = \frac{\dot{m}'_{\mathrm{TF}} - \dot{m}'_{core}}{\dot{m}'_{core}}. \quad \ldots (40)$$

Assuming that the turbofan core characteristics do not change, we can consider that the core specific power ($\mathrm{P}_{core}/\dot{m}_{core}$) is constant and equal to the one of the baseline configuration turbofans. Hence, the core mass flow can be calculated from the core power P'_{core} and the constant specific power as follows:

$$\dot{m}'_{core} = \frac{P'_{core}}{(\mathrm{P}_{core}/\dot{m}_{core})}. \quad \ldots (41)$$

Introducing Equation (41) into Equation (40), gives:

$$\mathrm{BPR} = \dot{m}'_{\mathrm{TF}} \cdot (\mathrm{P}_{core}/\dot{m}_{core})/P'_{core} - 1. \quad \ldots (42)$$

A simple iterative scheme is required for the resolution of Equations 38, 39 and 42. A first guess of the BPR allows the calculation of the underwing turbofan transmission efficiency with Equation (39), which is subsequently used to calculate the core power with Equation (38). A new BPR is then calculated with Equation (42) and the process continues until the BPR values converge.

Equation (38) highlights the main loss mechanism of this turbo-electric configuration, which counterbalances the BLI benefits; the higher the power sent to the BLI propulsor, the higher the losses due to the inefficiencies of the electric transmission chain. These additional losses tend to counteract the beneficial BLI effect of reducing the $P'_{K,\mathrm{BLIF}}$ term. It is highlighted to the reader that for constant core characteristics a change to the core exit power is directly translated to an equal change of fuel power. For a higher accuracy, the podded fan transmission efficiency can also be multiplied by a coefficient in order to add a degradation due to scaling effects, as a function of the core mass flow $\dot{m}_{core}$.

Having determined the impact on fuel power ($\Delta\mathrm{TSFC} \approx \Delta P_{core}$), the fuel burn evaluation can be completed by estimating the change in propulsion system drag and weight. Starting with the weight component, one needs to calculate the change in the under-wing turbofans weight and the added mass of the BLI propulsor. As the purpose of this paper is not to propose a new method of weight estimation, the reader is free to use whichever method they prefer. A few interesting methods, which would be compatible with the preliminary design approach developed in this work, are proposed by Guha et al[16] and Greitzer et al[17], and can be calibrated to better represent the designer's target. For this work, the mass of the underwing turbofans and of the BLI fan have been calculated as linear functions ($\mathrm{M} = a \cdot D_{fan} + b$) of their respective fan diameters, based on the detailed mechanical integration studies by Giannakakis et al[6]. With respect to the underwing turbofans, the correlation approximately

https://doi.org/10.1017/aer.2020.26 Published online by Cambridge University Press

Table 1
Validation case inputs

Parameter	Value
Altitude	35,000ft
Flight Mach	0.76
ΔISA	0K
Total thrust	39,000N
β	0.39
λ	0.41
q	0.33
Baseline Turbofan BPR	18.0
Under-wing fan hub/tip ratio	0.3
$\frac{V_{jet,\mathrm{TF}}}{V_0}$	1.29
D_{BLIF}	1.80m
$D_{\mathrm{BLIF},hub}$	0.60m
η_e	0.965
SP_e	3.14kW/kg

gives the variation in the weight of the low-pressure components and nacelle, as the core components weight stays fairly constant.

Subsequently, the total weight of the electric transmission chain is calculated by dividing the BLI fan power (estimated as $P'_{K,\mathrm{BLIF}}/\eta'_{fan,\mathrm{BLIF}}$) with the specific power of the transmission SP_e given in kW/kg.

Finally, the impact of the propulsion system drag change can be estimated by calculating the change in the propulsion system wetted area, based on the previously calculated propulsor diameters and assuming fixed length-to-diameter ratios.

The change in fuel burn at aircraft level is derived based on exchange rates given for the baseline aircraft configuration. The final fuel burn calculation is a linear combination of the fuel flow, weight and drag changes multiplied by appropriate exchange rates. It must be underlined that a different weight exchange rate has been used for the underwing and the rear installations.

$$\Delta \mathrm{FB} = \Delta \mathrm{TSFC} \cdot \mathrm{XR}_{\mathrm{TSFC}} + \Delta \mathrm{M} \cdot \mathrm{XR}_{\mathrm{M}} + \Delta \mathrm{S}_{\mathrm{W}} \cdot \mathrm{XR}_{\mathrm{S}}. \quad \ldots (43)$$

3.0 METHOD VALIDATION AND LIMITATIONS

The method described in the previous sections has been compared against the detailed preliminary design study published by the authors[6], in order to ascertain that it can produce reliable results for the design space exploration. The benchmark study included a full multipoint design and performance evaluation of the propulsion system, a CFD calculation of the flow ingested by the BLI fan and a mechanical design, integration and weight estimation of the propulsive system[6]. As such, it represents the most accurate estimation possible at a conceptual design stage and it can serve as a reliable benchmark for the validation of the analytical method presented herein.

The comparison takes place on the cruise point given in Table 1 together with the rest of the assumptions. According to the results of Giannakakis et al[6], the BLI fan produces 33%

https://doi.org/10.1017/aer.2020.26 Published online by Cambridge University Press

Table 2
Validation against the detailed study of Giannakakis et al[6]

	Predicted	Reference (6)
Δ TSFC	−3.5%	−4.0%
Δ Underwing turbofan diameter	−19%	−16%
Δ Propulsion system mass	+30%	+31%
Δ Fuel burn	+2.5%	+2.8%

of total thrust at cruise (30% at top-of-climb) and this is the value taken for the q parameter in Table 1. The turbofan BPR and average jet velocity $V_{jet,\mathrm{TF}}$ correspond to an Ultra High Bypass Ratio (UHBR) architecture. For simplification, the fan and low-pressure turbine efficiencies have been considered constant and equal to 0.94. A 2 pt efficiency penalty has been considered for the BLI fan which operates under distortion. A Coles velocity profile[18] has been assumed at the inlet of the BLI fan, with shape factor H equal to 1.4. The height of the boundary-layer is calculated iteratively in order to match the fuselage mechanical energy surface dissipation, i.e. $\Delta \mathrm{KE}\left(h'_{\mathrm{BLIF}}\right) = (\psi * F_N * V_0 * \beta/(\lambda + 1))$. The exchange rates used for the calculation correspond to a typical short- to medium-range aircraft and are the same as the ones used by Giannakakis et al[6].

The results of the verification are shown in Table 2, where one can readily see that the TSFC reduction predicted by the analytical method is sufficiently close to the higher fidelity estimation of Giannakakis et al[6]. Furthermore, the reduction in the underwing engines fan diameter is also predicted fairly accurately, leading to a good estimation of the propulsive system mass change. Finally, the change in fuel burn is also estimated with a satisfactory accuracy relative to the detailed study. Hence, overall the analytical method captures the correct trends, has satisfactory accuracy and can be used for the exploration exercises that follow.

The most important limitation of the analytical method is that it only evaluates the design on the cruise operating point and it is not capable of capturing multipoint design effects. For instance, an important multipoint design effect highlighted by the authors[6] concerned the operability of the underwing turbofans booster compressor, which operates close to surge at take-off, for a high BLI thrust contribution. That phenomenon can limit the thrust share of the BLI fan to about 30% of the total thrust.

4.0 RESULTS

4.1 Fuel burn optimisation and design space exploration for an SMR aircraft

The first step to a better understanding of what minimises the fuel burn of the turbo-electric architecture is the optimisation of the design parameters of the architecture for a given set of assumptions. More specifically, for the assumptions already given in Table 1 for an SMR class aircraft, Fig. 5 presents the optimisation of the BLI thrust share and diameter. It can readily be seen there is an optimum combination of BLI fan thrust and diameter that results in a minimum fuel burn increase of 1.9%. The optimum corresponds to 25% of thrust generated by the BLI propulsor and a BLI propulsor fan of 1.8m. As shown in Fig. 5, the existence of the above optimum BLI fan thrust and diameter can be explained by the variation of three principal

https://doi.org/10.1017/aer.2020.26 Published online by Cambridge University Press

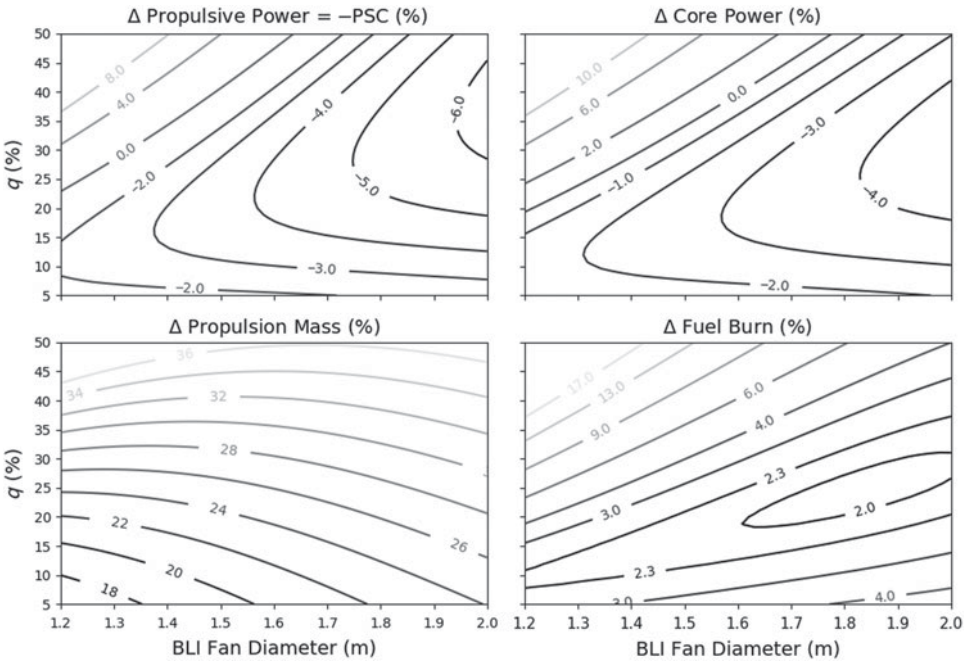

Figure 5. Fuel burn variation with D_{BLIF} and q.

factors: (1) the power saving coefficient, which is related to the BLI and propulsive efficiency benefits, (2) the core power variation which takes into account the transmission losses, (3) the change of propulsion system weight. These individual effects are detailed below.

Starting from the top left of Fig. 5, one can observe that for a given BLI fan diameter, the higher the thrust percentage q generated by the BLI propulsor, the higher the power saving. As discussed earlier with Fig. 3, this trend is expected as more thrust is being generated by a more efficient propulsor. Nonetheless, there is a certain BLI fan thrust threshold after which the PSC starts decreasing. In fact, increasing the BLI fan thrust for a given diameter, increases its jet velocity and after a point degrades its propulsive efficiency. For a given BLI fan thrust, increasing the diameter leads to more boundary-layer being ingested (increasing f in Fig. 3), up to the point where full ingestion occurs. After this threshold the power saving increases due to the decrease of jet velocities associated with the higher propulsor diameters (increasing α in Fig. 3), but only marginally.

The top right part of Fig. 5 also adds the effect of transmission losses between the propulsive kinetic energy requirement and the power at the exit of the turbofan cores. As a matter of fact, the variation of core power saving is very close to the PSC variation seen in top left of Fig. 5, with only one important difference. For a given diameter, the BLI fan thrust optimum is now lower due to the losses incurred in the transmission of power between the turbofans and the BLI fan.

Finally, the bottom left of Fig. 5 shows the propulsion system weight change, including the turbo-machinery and the electric components. According to the figure, for a constant BLI fan diameter, a higher BLI fan thrust leads to an increase in total weight due to the increasing weight of the electric components and the addition of the BLI propulsor weight, which outweigh the decrease in the size and mass of the underwing turbofans for the set of

https://doi.org/10.1017/aer.2020.26 Published online by Cambridge University Press

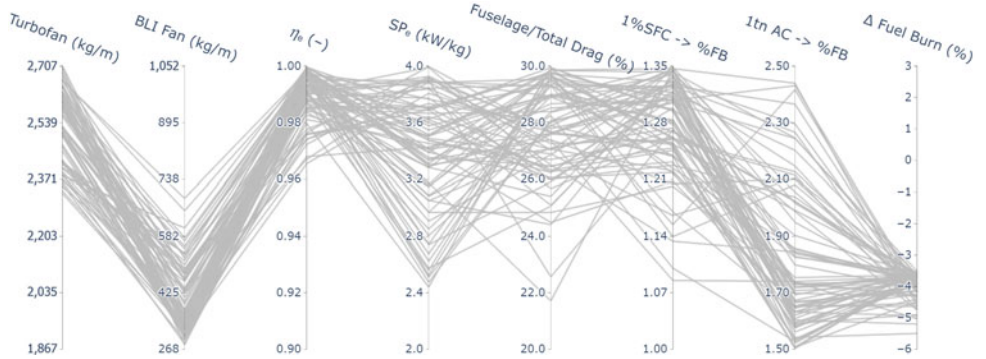

Figure 6. Exploration of the influence of different assumptions on the fuel burn change.

assumptions used for this optimisation. At a fixed BLI fan thrust, the weight increases with the increase in diameter of the BLI propulsor.

The estimated fuel burn change of +1.9% is in good agreement with the +1.7% estimated by the higher fidelity study carried out by the authors[6], but is nonetheless not on the same page with the fuel burn change of −3.4% claimed by Bowman et al[4]. Figure 6 tries to explain the variance in the results by exploring the impact that different assumptions have on fuel burn. Each line on the parallel coordinates graph represents an optimum design. Only the designs that give a fuel burn reduction higher than 3.5% are shown in order to isolate the common factors that lead to this result. A high concentration of lines for a given axis shows that the parameter of this axis is critical for achieving a fuel burn reduction; i.e. fuel burn is highly sensitive to this parameter.

The three factors that stand out the most are the underwing turbofan mass-to-diameter ratio, the same ratio for the BLI fan, and the efficiency of the electric transmission. If one uses underwing turbofans having a high mass-to-diameter ratio as a baseline, they have a better chance achieving a higher fuel burn reduction, as they benefit the most from the downsizing of the turbofans when $q > 0$. More precisely, what matters the most is the weight of the bypass flow components and nacelle, as these will be the ones that are going to be downsized. At the same time, aggressive assumptions need to be made regarding the installed BLI fan mass-to-diameter ratio. Future lightweight materials will have a positive impact on the BLI fan mass, but a negative one on the weight saving connected to the downsizing of the underwing turbofans. Figure 6 also shows that the BLI fan needs to be powered by an electric transmission with an efficiency higher than 96%, which is a condition that is quite difficult to satisfy with current electric machine technology. The authors have demonstrated that reducing the efficiency to about 91% would increase the fuel burn by about 0.4%[6]. Second in importance are the exchange rates that convert the change of TSFC and weight to a change of fuel burn. More particularly, a higher TSFC exchange rate and a lower weight rate, corresponding to longer range aircraft missions, would lead to a lower fuel burn. Next in importance is the ratio of fuselage drag to total aircraft drag, which needs to be higher than about 25% to produce a fuel burn reduction higher than 3.5%. Finally, a lightweight electric transmission with a high power density in terms of kW/kg is the last requirement identified by the exploration.

One can use the above conclusions in order to explain the different results found in the literature, i.e. −3.4% in fuel burn for Bowman et al[4] and +0.5% by Hall et al[5]. Bowman et al[4] use a fairly heavy turbofan baseline and a light BLI fan for their STARC-ABL study. According to the study of Welstead and Felder[3], which gives the preliminary results of the

https://doi.org/10.1017/aer.2020.26 Published online by Cambridge University Press

STARC-ABL aircraft, the underwing turbofan has a mass-to-diameter ratio of 2,135kg/m. At the same time the mass-to-diameter ratio of the BLI fan is on the light side with 456kg/m. On the other hand, the work by Hall et al[5] on the same aircraft architecture has underwing turbofans with a mass-to-diameter ratio of 1,601kg/m and a BLI fan at 828kg/m. These differences in mass assumptions can explain at least part of the disparity found in the fuel burn estimations of the two studies.

The above analysis demonstrates that the method presented in this paper is a powerful design space exploration tool when estimating the BLI potential at a conceptual design stage. The following section will shed more light on the parameters that influence the ratio of the ingested fuselage drag over the total aircraft and also show the importance of the propulsive efficiency of the conventional aircraft taken as baseline.

4.2 BLI potential for different aircraft applications

The objective of this section is to perform an evaluation of different aircraft types in terms of the ingested drag ratio f, which according to Figs 3 and 6 is directly related to the BLI power saving and to the minimisation of fuel burn. Given that f is a function of λ and β, these parameters need to be calculated for different aircraft applications. According to Equations (7) and (4), λ and β are related to the dissipation terms corresponding to the profile, vortex and wave drag losses. To enable their rapid computation based upon existing aircraft models, these parameters need to be expressed as a function of the aircraft drag contributions. Recalling Equation (32) and assuming for each aircraft analysed that $\beta_{fuselage} = 1.0$, i.e D'_{BLIF} is selected so that the complete boundary-layer of the fuselage is ingested, β is given by $C_{Dp,fuselage}/C_{Dp}$.

The ratio of the sum of the vortex and wave dissipation over the aircraft viscous mechanical power defect gives the following expression for λ:

$$\lambda = \frac{C_{Di} + C_{Dw}}{C_{Dp}} \quad \ldots (44)$$

with C_{Di} being the lift induced drag coefficient, C_{Dw} the wave drag coefficient and C_{Dp} the profile drag coefficient.

Replacing the above expression and $\beta = C_{Dp,fuselage}/C_{Dp}$ in Equation (9), one can calculate f as equal to $C_{Dp,fuselage}/C_D$, with C_D defined as:

$$C_D = C_{Dp} + C_{Di} + C_{Dw}. \quad \ldots (45)$$

The parameters β and f have been computed for in-house and published reference aircraft covering large business jet, commuter, regional, short-to-medium and long-range aircraft applications as shown in Table 3.

Figure 7 illustrates the analysed aircraft, along with lines representing constant values of λ. Aircraft applications featuring the highest value of f correspond to the largest potential BLI gains. Starting by ignoring the projected future aircraft indicated with the year entry-into-service (2035) and sorting the aircraft by BLI potential, one can observe that regional, commuter and short-to-medium aircraft come on top of the list. The large business jet segment ranks the lowest in terms of potential BLI gains.

When comparing λ for the different aircraft presented in Table 3, one must pay attention to the Mach number and C_L condition selected for the drag computation, which influence the wave and the vortex dissipation respectively. For instance, the aerodynamic performance of the LR was published for a Mach number of 0.80, while the values presented for the SMR

https://doi.org/10.1017/aer.2020.26 Published online by Cambridge University Press

Table 3
β and f data for conventional reference aircraft[a]

Category	Aircraft	Altitude	Mach	CL	β	f
Long-range	LR	35kft	0.80	0.55	0.37	0.22
Long-range	LR (2035)	35kft	0.80	0.55	0.41	0.27
Short-to-medium	SMR	35kft	0.76	0.55	0.39	0.25
Regional jet	RJ	36kft	0.75	0.50	0.30	0.22
Regional TP	RTP	23kft	0.50	0.50	0.29	0.25
Commuter TP	CTP	25kft	0.43	0.55	0.34	0.25
Commuter TP	CTP (2035)	25kft	0.43	0.55	0.38	0.29
Large business jet	BJ1	41kft	0.80	0.50	0.31	0.18
Large business jet	BJ2	36kft	0.80	0.50	0.29	0.15

[a] All aircraft data are based on in-house models apart from LR aircraft that are based on Isikveren et al[2] and CTP aircraft which are based on Fefermann et al[19].

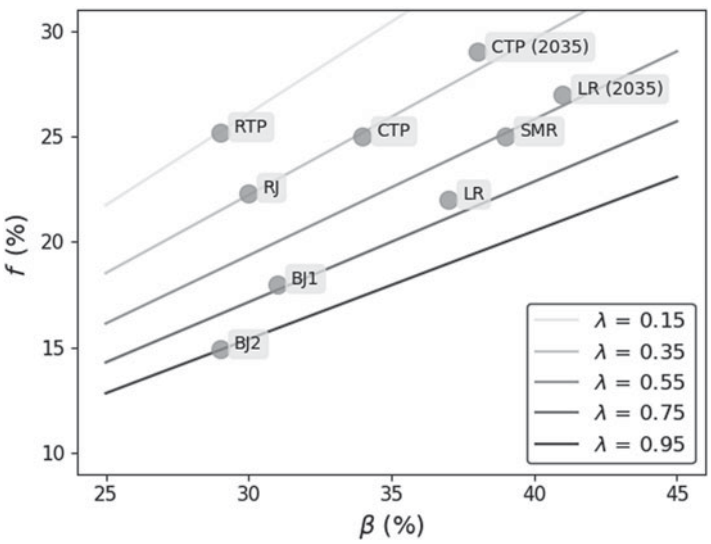

Figure 7. Aircraft analysis in terms of ingested to total drag ratio f.

were computed at a Mach number of 0.76. The larger wave dissipation due to the higher operating Mach number of the LR aircraft results in lower λ and consequently in a lower f value. The comparison of the operating C_L shows that the CTP was computed at $C_L = 0.55$ and the RTP at $C_L = 0.50$. As the vortex dissipation correlates with the square of C_L, the relative contribution of the vortex dissipation is higher in the case of the CTP, leading to a higher λ value relative to the RTP.

The large f value for turboprop commuter (CTP) and regional aircraft (RTP) is explained first by the fact that dissipation due to compressibility effects is around zero for an operating Mach number lower than 0.5. Consequently, the term λ does not include any wave dissipation contribution. In addition, high wing aspect ratios are achieved with the thick, straight

https://doi.org/10.1017/aer.2020.26 Published online by Cambridge University Press

trapezoidal wing design of turboprop aircraft. Consequently, vortex dissipation is lower as it is inversely correlated to the wing aspect ratio, leading finally to a lower value of λ. However, it should be underlined that the f value of both turboprop aircraft is based on an unpowered high-speed polar (propeller feathered/stopped glide drag polar). Hence, the impact of thrust on the aircraft drag (propeller wake and wing interaction) is not considered. Taking into account the increase in drag due to presence of the propellers would tend to slightly increase λ, which would subsequently decrease f, i.e. the BLI potential benefit. The regional jets share similar β values with regional turboprops, however their λ includes a wave drag dissipation contribution due to the higher operating Mach number. Moreover, the slender, swept wing design of regional jets results in lower achievable aspect ratio and consequently higher vortex dissipation. Similar reasoning is applied when comparing the positioning of large business jet towards larger values of λ. Operating in the high-end of the transonic speed region with Mach numbers between 0.85 and 0.9, the contribution of the wave drag dissipation increases. The contribution of vortex and wave dissipation results in larger values of λ, which relatively reduces the contribution of the fuselage viscous dissipation over the total aircraft dissipation and the potential BLI benefits.

When comparing the β values, short-to-medium and long-range aircraft show values of around 40%, while business jet and regional aircraft demonstrate values of around 30%. This trend indicates that the contribution of the viscous dissipation of the fuselage over the total aircraft dissipation increases when going towards larger transport aircraft. The geometrical dimensions of the fuselage and the resulting fuselage wetted area are directly correlated to the viscous dissipation. A rising passengers number should also increase β, as the fuselage dimensions are determined primarily by the cabin layout designed to accommodate the number of passengers.

When considering the projected future aircraft in the analysis, the increase in f compared to the state-of-the-art aircraft indicates that the integration of future advanced technologies strengthens the case for propulsion featuring fuselage BLI. Advanced technologies that target the reduction in vortex and wave dissipation tend to make the case for propulsive fuselage more attractive, as they increase the relative contribution of the fuselage viscous dissipation over the total aircraft power defect. By comparing the LR and the projected LR (2035)[20], a 10% and a 23% increase in β and f are found respectively, while λ is reduced from 0.7 to 0.5. The significant change in β is related to the increase in fuselage length by 5% and in diameter by 13%, in order to reflect the higher demand for aircraft cabin comfort and the change in passenger anthropometry[21]. In this case, the increase in $C_{Dp,fuselage}$ due to the geometrical dimensions change was partially counteracted by the introduction of riblets on the fuselage surface to reduce viscous dissipation. The reduction in λ is explained by the introduction of an advanced very flexible wing, with an aspect ratio increased by 35%, leading to a reduction in vortex dissipation. Moreover, shock contour bumps were implemented on the wing upper surface to reduce wave dissipation. These reductions in dissipation explain the change in λ. The same reasoning applies for the CTP and the projected CTP (2035)[19].

However, the above analysis only considered the maximum ingested fuselage dissipation as the metric representing the BLI potential. As shown by Fig. 3, aircraft with high baseline $\frac{V_{jet}}{V_0}$ are good candidates for installing a BLI propulsion due to their low initial propulsive efficiency. This hypothesis is confirmed by Fig. 8 that shows the estimated values of PSC for the aforementioned aircraft using the following simplifying assumptions:

- 30% of total thrust is generated by the BLI propulsor, i.e. $q = 0.30$.
- The podded turbofans maintain the same jet velocity, i.e. $\frac{V'_{jet,\mathrm{TF}}}{V_0} = \frac{V_{jet,\mathrm{TF}}}{V_0}$.

https://doi.org/10.1017/aer.2020.26 Published online by Cambridge University Press

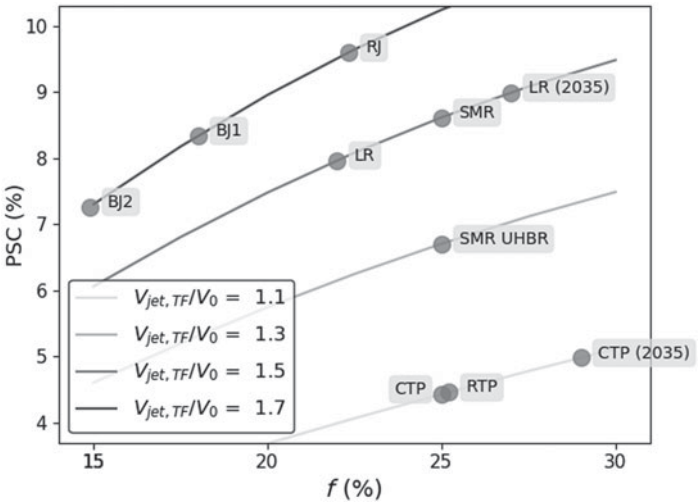

Figure 8. Aircraft analysis in terms of PSC.

- No increase of total mass flow between the BLI and conventional configurations, i.e. $\alpha = 1$.
- Typical jet velocity ratios:
  - RTP, CTP, CTP (2035): $\frac{V_{jet,\mathrm{TF}}}{V_0} = 1.1$.
  - SMR with UHBR engines: $\frac{V_{jet,\mathrm{TF}}}{V_0} = 1.3$.
  - SMR, LR, LR (2035): $\frac{V_{jet,\mathrm{TF}}}{V_0} = 1.5$.
  - RJ, BJ1, BJ2: $\frac{V_{jet,\mathrm{TF}}}{V_0} = 1.7$.

According to the results shown in Fig. 8, the application of propulsive fuselage on baseline aircraft equipped with moderate efficiency turbofans, such as the regional jet RJ, is favored against applications currently using turboprop engines, even though the latter have significantly higher ingested drag values f. As a matter of fact, turboprops provide the worst BLI potential saving, despite their first in class ingested drag ratios. The best in class RJ aircraft, is followed by the 2035 LR and the current technology SMR aircraft, while the current technology LR is just behind. It should be noted that a 2035 SMR aircraft would probably rank higher than the equivalent 2035 LR. Although the business jet aircraft also demonstrate high PSC, the location of the podded turbofans near the tail imposes severe space restrictions to the installation of the propulsive fuselage fan. Finally, having a UHBR engine as a baseline, already results in low jet velocity and high propulsive efficiency and leads to reduced potential power saving through BLI, as shown by the SMR UHBR point of Fig. 8.

5.0 CONCLUSIONS

An analytical method based on the evaluation of mechanical energy dissipation was developed in order to estimate the potential of advanced propulsion systems featuring BLI. In particular, the method aimed at assessing the BLI benefits of a turbo-electric propulsive fuselage concept. The method treats the system integration impact of a propulsive fuselage fan at aircraft level and determines the potential fuel burn reduction. The design space exploration showed that

https://doi.org/10.1017/aer.2020.26 Published online by Cambridge University Press

the assumptions regarding the underwing turbofans and BLI fan mass estimation can have an important impact on the final fuel burn estimation. The same applies to the total efficiency assumed for the electric transmission, the range of the aircraft mission, and the propulsive efficiency of the engines used as benchmark.

It was shown that the regional jet and short- to medium-range aircraft classes are the most promising as the ingested drag and power saving are among the largest, with long-range aircraft being just behind. Turboprop aircraft would be less appropriate candidates, despite their high-ingested drag potential, due to their existing highly efficient propellers. The future introduction of advanced technologies, which target the reduction of vortex and wave dissipation at aircraft level, could increase the potential benefit of propulsive fuselage BLI. On the other hand, the potential benefit would be decreased if more efficient and lighter ultra-high bypass ratio engines were used as benchmark.

ACKNOWLEDGEMENTS

The authors would like to thank Dr. Askin Isikveren, Nicolas Tantot and Benoit Rodriguez for all the fruitful discussions on the topic of turbo-electric BLI architectures. The authors would also like to thank the journal reviewers for their help in improving the overall clarity and quality of the paper. This work has received funding from the Clean Sky 2 Joint Undertaking under the European Union's Horizon 2020 research and innovation program under the contract CS2-LPA-GAM-2018-01.

REFERENCES

1. Advisory Council for Aviation Research and Innovation in Europe, Strategic Research & Innovation Agenda, Volume 1, 2017.
2. ISIKVEREN, A.T., SEITZ, A., BIJEWITZ, J., MIRZOYAN, A., ISYANOV, A., GRENON, R., ATINAULT, O., GODARD, J.-L and STÜCKL, S. Distributed propulsion and ultra-high by-pass rotor study at aircraft level, *The Aeronautical Journal*, 2015, **119**, pp 1327–1376.
3. WELSTEAD, J. and FELDER, J. Conceptual design of a single-aisle turboelectric commercial transport with fuselage boundary layer ingestion, 54th AIAA Aerospace Sciences Meeting, AIAA SciTech Forum, no. AIAA 2016-1027, 2016.
4. BOWMAN, C.L., FELDER, J.L. and MARIEN, T.V. Turbo- and hybrid-electrified aircraft propulsion for commercial transport, AIAA/IEEE Electric Aircraft Technologies Symposium, AIAA Propulsion and Energy Forum, 2018.
5. HALL, D.K., DOWDLE, A.P., GONZALEZ, J.J., TROLLINGER, L. and THALHEIMER, W. Assessment of a boundary layer ingesting turboelectric aircraft configuration using signomial programming, Aviation Technology, Integration, and Operations Conference, AIAA Aviation Forum, 2018.
6. GIANNAKAKIS, P., MALDONADO, Y.-B, TANTOT, N., FRANTZ, C. and BELLEVILLE, M. Fuel burn evaluation of a turbo-electric propulsive fuselage aircraft, AIAA Propulsion and Energy Forum, Indianapolis, IN, August 2019.
7. DRELA, M. Power balance in aerodynamic flows, *AIAA Journal*, 2009, **47**, (7), pp 1761–1771.
8. SATO, S. The Power Balance Method for Aerodynamic Performance Assessment, PhD thesis, Massachusetts Institute of Technology, 2012.
9. HALL, D.K., HUANG, A.C., URANGA, A., GREITZER, E.M., DRELA, M. and SATO, S. Boundary layer ingestion propulsion benefit for transport aircraft, *Journal of Propulsion and Power*, 2017, **33**, (5), pp 1118–1129.
10. URANGA, A., DRELA, M., GREITZER, E.M., HALL, D.K., TITCHENER, N.A., LIEU, M.K., SIU, N.M., CASSES, C., HUANG, A.C., GATLIN, G.M. and HANNON, J.A. Boundary layer ingestion benefit of the D8 transport aircraft, *AIAA Journal*, 2017, **55**, (11), pp 3693–3708.

https://doi.org/10.1017/aer.2020.26 Published online by Cambridge University Press

11. SMITH, L.H. Wake ingestion propulsion benefit, *Journal of Propulsion and Power*, 1993, **9**, (1), pp 74–82.
12. STEINER, H.-J, SEITZ, A., WIECZOREK, K., PLÖTNER, K., ISIKVEREN, A.T. and HORNUNG, M. Multidisciplinary design and feasibility study of distributed propulsion systems, 28th International Congress of the Aeronautical Sciencies, no. Paper ICAS 2012-1.7.5, September 2012.
13. HALL, D.K. Analysis of Civil Aircraft Propulsors with Boundary Layer Ingestion,. PhD thesis, Massachusetts Institute of Technology, 2015.
14. FELDER, J., KIM, H., BROWN, G. and KUMMER, J. An examination of the effect of boundary layer ingestion on turboelectric distributed propulsion systems, 49th AIAA Aerospace Sciences Meeting including the New Horizons Forum and Aerospace Exposition, Aerospace Sciences Meetings, AIAA, January 2011.
15. GIANNAKAKIS, P., LASKARIDIS, P. and PILIDIS, P. Effects of off-takes for aircraft secondary-power systems on jet engine efficiency, *Journal of Propulsion and Power*, 2011, **27**, (5), pp 1024–1031.
16. GUHA, A., BOYLAN, D. and GALLAGHER, P. Determination of optimum specific thrust for civil aero gas turbine engines: a multidisciplinary design synthesis and optimisation, *Proceedings of the Institution of Mechanical Engineers, Part G: Journal of Aerospace Engineering*, 2013, **227**, (3), pp 502–527.
17. GREITZER, E.M., BONNEFOY, P., DELAROSABLANCO, E., DORBIAN, C., DRELA, M., HALL, D., HANSMAN, R., HILEMAN, J., LIEBECK, R., LOVEGREN, J., MODY, P., PERTUZE, J., SATO, S., SPAKOVSZKY, Z., TAN, C., HOLLMAN, J., DUDA, J., FITZGERALD, N., HOUGHTON, J., KERREBROCK, J., KIWADA, G., KORDONOWY, D., PARRISH, J., TYLKO, J., Wen, AND LORD, W. N+ 3 aircraft concept designs and trade studies. volume 2: appendices-design methodologies for aerodynamics, structures, weight, and thermodynamic cycles, Tech Rep CR 2010-216794, NASA, 2010.
18. COLES, D. The law of the wake in the turbulent boundary layer, *Journal of Fluid Mechanics*, 1956, **1**, (2), pp 191–226.
19. FEFERMANN, Y., MAURY, C., LEVEL, C., ZARATI, K., SALANNE, J.-P, PORNET, C., THORAVAL, B. and ISIKVEREN, A. Hybrid-electric motive power systems for commuter transport applications, 30th Congress of the International Council of the Aeronautical Sciences (ICAS), No. ICAS-2016-0438, Daejeon, Korea, 2016.
20. BIJEWITZ, J., SEITZ, A., ISIKVEREN, A.T. and HORNUNG, M. Multi-disciplinary design investigation of propulsive fuselage aircraft concepts, *Aircraft Eng & Aerospace Tech*, 2016, **88**, pp 257–267.
21. SCHMIDT, M., PLÖTNER, K.O., PORNET, C., ISIKVEREN, A.T. and HORNUNG, M. Contributions of cabin related and ground operation technologies towards flightpath 2050, Deutscher Luft- und Raumfahrtkongress 2013 (DGLR), No. Paper 301299, Stuttgart, Germany, September 2013.

https://doi.org/10.1017/aer.2020.26 Published online by Cambridge University Press